Accuracy of elastic finite differences in smooth media

Luděk Klimeš

Department of Geophysics, Charles University, Ke Karlovu 3, 121 16 Praha 2, Czech Republic, E-mail: klimes@seis.karlov.mff.cuni.cz

Abstract

The accuracy of finite–difference schemes of the 2^{nd} and 4^{th} order in 2-D and 3-D regular rectangular grids is studied. The method of designing the schemes and estimating their accuracy is proposed. The paper is devoted to the point schemes, expressed in terms of the discretized (point) values of the wavefield and material parameters. Only the common schemes applicable in smooth parts of seismic models, outside structural interfaces, are taken into account. Finite differences at structural interfaces are studied elsewhere.

The inaccuracy of finite–difference schemes is governed, above all, by the error in the phase velocity, caused by discretization. This error is estimated for several finite–difference schemes. It is explicitly dependent on the direction of propagation and on wave polarization. The maximum phase–velocity error over all directions of propagation enables the accuracy of the individual schemes to be appreciated in order to select the best one. The proposed approach is general and applicable to other finite–difference schemes, for example, of the 6^{th} and higher orders.

Keywords

Seismic waves, finite differences of the 2^{nd} and 4^{th} order, 2-D and 3-D seismic modelling, accuracy, elasticity.

1 Introduction

The accuracy of finite–difference schemes of the 2^{nd} and 4^{th} order in 2-D and 3-D regular rectangular grids is studied in this paper. Only the point schemes, expressed in terms of the discretized (point) values of the wavefield and material parameters, are considered. Since this paper is devoted to finite–difference calculation of *elastic waves*, the word *wavefield* will stand for space–time dependent *displacement vector* throughout this paper.

Since the finite grid spacing causes the most severe problems at the highest frequencies contained within the waveforms, we concentrate especially on the high–frequency behaviour of finite–difference schemes. From this point of view, the optimum finite–difference schemes built on a given small neighbourhood of each point are the schemes designed by means of truncated Taylor expansions. We consider *centred* (sometimes also called *conventional*, e.g. by Stephen 1988) point finite–difference schemes of the 2^{nd} and 4^{th} order with all wavefield values and material parameters specified or calculated at the gridpoints, and *staggered* schemes of the 2^{nd} and 4^{th} order according to Madariaga (1976), Virieux and Madariaga (1982), Virieux (1986), Levander (1988) and Sei (1993), with wavefield values calculated half way between gridpoints along the corresponding gridlines, the diagonal stress components evaluated at the gridpoints and

Pure appl. Geophys., 148 (1996), 39–76.

the mixed stress components evaluated at the centres of the square faces formed by the corresponding gridlines.

In Sections 2 and 3, the method of designing the centred point finite–difference schemes applicable in smooth parts of seismic models, outside structural interfaces, is presented. The method is suitable both in isotropic and anisotropic seismic models. The schemes have a general form of linear operators acting on the wavefield grid values. These finite–difference schemes may be generalized for application in the vicinity of structural interfaces. The application at structural interfaces is presented elsewhere in order to keep this paper concise and readable.

In Sections 4 and 5, the tools for estimating the accuracy of finite–difference schemes are presented. The harmonic wavefield is *locally* considered to be composed of P and S waves propagating with the corresponding *phase velocities*. The inaccuracy of finite–difference schemes is governed especially by the error in the phase velocity, caused by discretization. The presented methods for estimating the accuracy of finite–difference schemes are applicable both to isotropic and anisotropic seismic models.

Section 6 gives the accuracy and some other properties of several particular finite–difference approximations of individual partial wavefield derivatives ("partial schemes"). This analysis follows the method of Sections 2 and 3. The wavefield finite differencing is, of course, independent of anisotropy.

In Section 7, the relative phase–velocity error due to the inaccurate second partial wavefield derivatives in isotropic models is estimated. This error is estimated for several finite–difference schemes of the 2^{nd} and 4^{th} order in 2-D and 3-D regular rectangular grids. It is explicitly dependent on the direction of propagation and on wave polarization. The maximum phase–velocity error over all directions of propagation enables the accuracy of individual schemes to be appreciated in order to find the best one. Section 7 follows from Sections 5 and 6.

In Section 8, the relative phase–velocity error due to the inaccurate first partial wavefield derivatives is estimated.

In Section 9, the relative phase–velocity error due to the inaccurate first partial derivatives of the material parameters is estimated.

In Section 10, the relative phase–velocity error of the staggered finite–difference schemes due to the inaccurate values of the material parameters is briefly discussed.

The proposed approach is general and applicable to other finite–difference schemes, for example, of the 6^{th} and higher orders.

2 Wavefield on a rectangular grid

Expressions of this Section are in the first place devoted to the centred finite–difference schemes, but they should also be applicable to other (e.g., staggered) point finite–difference schemes with only minor modifications.

2.1 Gridpoints and discretization

At a fixed time, the wavefield is represented by grid values $u_i(\mathbf{x})$, where the positional vector $\mathbf{x}$ takes the values (positions) of all gridpoints. In the computer memory, the gridpoints are, as a rule, indexed. The positional vector $\mathbf{x}$ is then represented by the corresponding integer index, and $u_i(\mathbf{x})$ by an array.

Denote by $\mathbf{h}_i$ the vectorial grid intervals. If the grid is regular and rectangular in Cartesian coordinates, and the grid intervals are of the same length h in all directions, we may choose

$$\mathbf{h}_1 = (h,0,0)^{\mathrm{T}} \ , \quad \mathbf{h}_2 = (0,h,0)^{\mathrm{T}} \ , \quad \mathbf{h}_3 = (0,0,h)^{\mathrm{T}} \quad . \tag{1}$$

Gridpoints $\mathbf{y}$, from the vicinity of fixed gridpoint $\mathbf{x}$ situated inside the grid, may then be expressed as

$$\mathbf{y} = \mathbf{x} + n_1\mathbf{h}_1 + n_2\mathbf{h}_2 + n_3\mathbf{h}_3 = \mathbf{x} + n_i\mathbf{h}_i \quad , \tag{2}$$

where n_1, n_2, and n_3 are small whole numbers (integers). For instance, $n_i = -1,0,1$ for 3-D finite differences of the second order, and $n_I = -1,0,1$, $n_3 = 0$ for 2-D finite differences of the second order. If the gridpoints are indexed, grid intervals $\mathbf{h}_1$, $\mathbf{h}_2$, $\mathbf{h}_3$ are represented by the corresponding shifts of the index.

2.2 Taylor expansion

For fixed gridpoint $\mathbf{x}$ situated inside the grid, we put

$$u_{i(n_1,n_2,n_3)} = u_i(\mathbf{x} + n_1\mathbf{h}_1 + n_2\mathbf{h}_2 + n_3\mathbf{h}_3) \quad . \tag{3}$$

These grid values are the arguments of a linear finite–difference operator. Within a smooth geological block, the grid values may be approximated by a Taylor expansion from gridpoint $\mathbf{x}$.

Let us denote the value and partial derivatives of the wavefield at $\mathbf{x}$ by

$$\begin{aligned}
& U_i = u_i(\mathbf{x}) \ , \quad U_{ij} = u_{i,j}(\mathbf{x}) = \frac{\partial u_i}{\partial x_j}(\mathbf{x}) \ , \quad U_{ijk} = u_{i,jk}(\mathbf{x}) = \frac{\partial^2 u_i}{\partial x_j \partial x_k}(\mathbf{x}) \ , \\
& U_{ijkl} = u_{i,jkl}(\mathbf{x}) = \frac{\partial^3 u_i}{\partial x_j \partial x_k \partial x_l}(\mathbf{x}) \ , \\
& U_{ijklm} = u_{i,jklm}(\mathbf{x}) = \frac{\partial^4 u_i}{\partial x_j \partial x_k \partial x_l \partial x_m}(\mathbf{x}) \ , \quad \ldots \quad .
\end{aligned} \tag{4}$$

Grid values (3) may then be approximated by

$$u_{i(n_1,n_2,n_3)} = U_i + hU_{ij}n_j + \frac{h^2}{2}U_{ijk}n_jn_k + \frac{h^3}{6}U_{ijkl}n_jn_kn_l + \frac{h^4}{24}U_{ijklm}n_jn_kn_ln_m + \ldots \ . \tag{5}$$

For fixed $\mathbf{x}$, grid values (3) are arranged into vector $\mathbf{u}$, and partial derivatives (4) into vector $\mathbf{U}$. It means that all considered combinations of the indices of $u_{n(n_1,n_2,n_3)}$ are ordered in some way (e.g., $_{1(-2,-2,-2)}$, $_{2(-2,-2,-2)}$, $_{3(-2,-2,-2)}$, $_{1(-1,-2,-2)}$, $\ldots$, $_{3(2,2,2)}$), and that each combination $_{n(n_1,n_2,n_3)}$ represents a single index in vector $\mathbf{u}$. Equal derivatives (e.g., U_{112} and U_{121}) are summed to form a single element of $\mathbf{U}$ (e.g., $U_{1[12]} =$

$U_{112}+U_{121}$, where index $[i,j]$ corresponds to all permutations of i and j). It means that the spatial wavefield derivatives are represented by components $U_{i[jk...]}$. All considered combinations of the indices of $U_{i[jk...]}$ are ordered in some way (e.g., $_1$, $_2$, $_3$, $_{1[1]}$, $_{2[1]}$, ..., $_{1[11]}$, $_{2[11]}$, ...), and each combination $_{i[j,k,...]}$ represents a single index in vector $\mathbf{U}$.

Taylor expansion (5) may then be expressed as the linear transformation

$$\mathbf{u} = \mathbf{T}\mathbf{U} \quad , \tag{6}$$

where the elements of Taylor–expansion matrix $\mathbf{T}$, projecting U_i, $U_{i[j]}$, $U_{i[jk]}$, $U_{i[jkl]}$, $U_{i[jklm]}$, ... onto $u_{n(n_1,n_2,n_3)}$, are

$$\begin{aligned}
T_{n(n_1,n_2,n_3):i} &= \delta_{ni} \ , \\
T_{n(n_1,n_2,n_3):i[j]} &= \delta_{ni} h n_j \ , \\
T_{n(n_1,n_2,n_3):i[jk]} &= \delta_{ni} \frac{h^2}{2} n_j n_k \ , \\
T_{n(n_1,n_2,n_3):i[jkl]} &= \delta_{ni} \frac{h^3}{6} n_j n_k n_l \ , \\
T_{n(n_1,n_2,n_3):i[jklm]} &= \delta_{ni} \frac{h^4}{24} n_j n_k n_l n_m \ , \quad \dots \quad .
\end{aligned} \tag{7}$$

The combinations representing the first index and the second index of each element of $\mathbf{T}$ are separated by a colon.

2.3 Evaluation of the second time derivatives of the wavefield from the elastodynamic equations

Let us consider general linear stress–strain relations

$$\sigma_{ij} = c_{ijkl} u_{k,l} \quad , \tag{8}$$

where c_{ijkl} are the elastic parameters (stiffnesses). In an isotropic medium,

$$c_{ijkl} = \delta_{ij}\delta_{kl}\lambda + \delta_{ik}\delta_{jl}\mu + \delta_{il}\delta_{jk}\mu \tag{9}$$

with

$$\lambda = \rho({v_\mathrm{P}}^2 - 2{v_\mathrm{S}}^2) \ , \quad \mu = \rho {v_\mathrm{S}}^2 \quad . \tag{10}$$

The second partial time derivative of the wavefield is given by the elastodynamic equation

$$u_i'' = \rho^{-1} \frac{\partial \sigma_{ij}}{\partial x_j} = \rho^{-1}(c_{ijkl} u_{k,lj} + c_{ijkl,j} u_{k,l}) \quad , \tag{11}$$

and specifically at $\mathbf{x}$

$$u_i''(\mathbf{x}) = \rho^{-1}(C_{ijkl} U_{klj} + C_{ijklj} U_{kl}) \quad , \tag{12}$$

where

$$C_{ijkl} = c_{ijkl}(\mathbf{x}) \ , \quad C_{ijklm} = \frac{\partial c_{ijkl}}{\partial x_m}(\mathbf{x}) \tag{13}$$

are the values and partial derivatives of the elastic parameters at central point $\mathbf{x}$. In an isotropic medium,

$$C_{ijkl}U_{klj} = (\lambda + \mu)\, U_{kki} + \mu U_{ikk} \quad , \tag{14}$$

$$C_{ijklj} = \delta_{kl}\frac{\partial\lambda}{\partial x_i}(\mathbf{x}) + \delta_{il}\frac{\partial\mu}{\partial x_k}(\mathbf{x}) + \delta_{ik}\frac{\partial\mu}{\partial x_l}(\mathbf{x}) \quad , \tag{15}$$

and

$$C_{ijklj}U_{kl} = \frac{\partial\lambda}{\partial x_i}(\mathbf{x})\; U_{kk} + \frac{\partial\mu}{\partial x_k}(\mathbf{x})\;\; [U_{ik} + U_{ki}] \quad . \tag{16}$$

Partial derivatives C_{ijklm} of the elastic parameters at $\mathbf{x}$ may be approximated using symmetrical differences

$$C_{ijklm} = \frac{1}{2h}[c_{ijkl}(\mathbf{x} + \mathbf{h}_m) - c_{ijkl}(\mathbf{x} - \mathbf{h}_m)] \tag{17}$$

of the second order if all points $\mathbf{x} - \mathbf{h}_m$, $\mathbf{x}$, $\mathbf{x} + \mathbf{h}_m$ are situated in the same geological block. In other words, if the points are not separated by a structural interface. At structural interfaces, partial derivatives C_{ijklm} should preferably be calculated by model–specification software instead of differencing.

Equation (12) expresses the linear dependence

$$\mathbf{t} = \mathbf{S}\mathbf{U} \tag{18}$$

of vector

$$\mathbf{t} = (u_1'', u_2'', u_3'')^{\mathrm{T}} \tag{19}$$

on the vector $\mathbf{U}$ of the partial derivatives. The only nonzero components of matrix $\mathbf{S}$ are

$$S_{n:i[j]} = \rho^{-1}C_{ijnkk} \ , \quad S_{n:i[jk]} = \rho^{-1}(C_{ijkn} + C_{ikjn})/2 \quad , \tag{20}$$

projecting $U_{i[j]}$ and $U_{i[jk]}$ onto u_n'', respectively. The combinations representing the first index and the second index of each element of $\mathbf{S}$ are separated by a colon.

3 Finite–difference schemes inside geological blocks

To determine the spatial finite–difference scheme for a fixed time, we select N wavefield values at the gridpoints within the vicinity of each central point $\mathbf{x}$. These N values determine vector $\mathbf{u}$ of the wavefield grid values. Equation (6) then represents N linear equations for the partial wavefield derivatives arranged in vector $\mathbf{U}$. We thus have to select N nonzero partial derivatives and put all other components of $\mathbf{U}$ equal to zero. The partial wavefield derivatives up to the second order must not be annulled. The set of N nonzero components of $\mathbf{U}$ has to be selected so that the resulting system (6) of N linear equations for N nonzero components of $\mathbf{U}$ is regular. Thus, in our approach, the finite–difference scheme will be fully determined by selecting the set of N grid wavefield values (arguments of the scheme) and the set of N nonzero partial wavefield derivatives.

If a reasonable subset $\mathbf{u}$ of grid values (3) and the corresponding reasonable subset $\mathbf{U}$ of partial derivatives (4) is chosen, Taylor–expansion matrix $\mathbf{T}$ may be inverted and equation (6) can be solved,

$$\mathbf{U} = \mathbf{T}^{-1}\mathbf{u} \quad . \tag{21}$$

Particular grid values (3) contained within vector $\mathbf{u}$ and partial derivatives (4) contained within vector $\mathbf{U}$ leading to each partial finite–difference scheme considered are given in Section 6, see e.g., (49) and (50) for the partial finite–difference scheme of Section 6.1. Vectors $\mathbf{u}$ and $\mathbf{U}$ leading to each finite–difference scheme considered in Section 7 are composed of the components corresponding to all partial schemes of which the finite–difference scheme is assembled.

From (7) it is obvious that the inverse Taylor–expansion matrix $\mathbf{T}^{-1}$ depends only on the grid structure and on the selected size and structure of vectors $\mathbf{u}$ and $\mathbf{U}$, i.e. on the choice of the finite–difference scheme. Moreover, for a regular grid, the inverse Taylor–expansion matrix $\mathbf{T}^{-1}$ is the same for all "inner" gridpoints $\mathbf{x}$. The finite–difference schemes of "inner" gridpoints do not cross the grid boundaries or structural interfaces.

The finite–difference scheme inside a smooth geological block may now be expressed in the general matrix form of

$$\mathbf{t} = \mathbf{S}\mathbf{T}^{-1}\mathbf{u} \quad . \tag{22}$$

4 Accuracy of finite–difference schemes — basic concepts

4.1 Errors

Error $\delta(Q)$ of quantity Q is understood hereinafter as the deviation of the approximate value Q from value $\bar{Q}$ corresponding to the exact solution of the relevant equations,

$$\delta(Q) = Q - \bar{Q} \quad . \tag{23}$$

4.2 Asymptotic approximation of wavefield derivatives

First we introduce the parameters describing grid spacing with respect to the wavelength,

$$\epsilon_0 = -\mathrm{i}\frac{2\pi H}{T} \quad , \quad \epsilon = \mathrm{i}\frac{2\pi h}{\Lambda} \quad , \tag{24}$$

where H is the time step, h is the grid interval in space, T is the period, and Λ is the wavelength of a monochromatic wave. We also denote

$$\epsilon_i = \epsilon \vartheta_i \quad , \tag{25}$$

where ϑ_i are the components of the unit vector normal to the wavefront. The partial wavefield derivatives may then be roughly approximated at high frequencies by

$$u_i'' \simeq u_i \left(-\mathrm{i}\frac{2\pi}{T}\right)^2 = u_i \left(\frac{\epsilon_0}{H}\right)^2 = u_i \left(\frac{v\epsilon}{h}\right)^2 \quad , \tag{26}$$

and

$$U_{ijk...n} \simeq U_i \frac{\epsilon_j}{h}\frac{\epsilon_k}{h} ... \frac{\epsilon_n}{h} \quad . \tag{27}$$

We have denoted by $u_i'' = \partial^2 u_i / \partial t^2$ the second partial wavefield derivative with respect to time.

4.3 Relative phase–velocity error

The error of the calculated wavefield is caused by the inaccuracy of the evaluation of the second derivative u_i'' of the wavefield with respect to time by means of the finite-differences in space, and by the inaccuracy of the finite–difference scheme of the second order along the time axis.

Error $\delta(u_i'')$ in the second derivative u_i'' of the harmonic wave of a particular polarization has approximately the same effect on the wave propagation as a perturbation of the elastic parameters causing the perturbation

$$\delta(\Gamma_{ik}) = \frac{\delta(u_i'')u_k}{u_m'' u_m} \tag{28}$$

of the Christoffel matrix

$$\Gamma_{ik} \simeq \rho^{-1} C_{ijkl} \frac{\epsilon_j \epsilon_l}{v^2 \epsilon^2} \quad . \tag{29}$$

Let us emphasize that the zero–order ray approximation is used here just to locally estimate the influence of small error $\delta(u_i'')$ in the second wavefield derivative on the wave propagation, not to approximate the calculated wavefield. Equation (29) is thus only displayed for reader's convenience and is not used here.

The *principal component* of error $\delta(u_i'')$ in the second derivative u_i'' is the component along the polarization vector

$$e_i = U_i / \sqrt{U_m U_m} \quad . \tag{30}$$

The principal component of error $\delta(u_i'')$ influences the corresponding eigenvalue of the Christoffel matrix and consequently the phase velocity. This error, $e_i \delta(u_i'')$, thus influences the calculated wavefield considerably. Its real part causes the error in the phase velocity along the ray and, consequently, in travel time, whereas its imaginary part causes the errors in the amplitude of the calculated waves. Let us emphasize that the imaginary part of the principal component of the error in u_i'' causes the same corresponding relative deviation from the exact solution as does the real part of the same magnitude.

The *additional components* of error $\delta(u_i'')$ in the second derivative u_i'' are perpendicular to polarization vector e_i. They influence the eigenvectors of the Christoffel matrix but not its eigenvalues. The additional components of error $\delta(u_i'')$ in second derivative u_i'' thus locally disturb the polarization of the wavefield, but have no considerable influence on the phase velocity or on the magnitude of the wavefield amplitudes, as compared with the influence of the principal component of the error. As opposed to the principal component, the additional components of the error do not accumulate during wave propagation, with the exception of S waves in an isotropic medium, where the additional components of the error cause the frequency–dependent cumulative rotation of the polarization vectors. Although the final error in the vectorial amplitudes of S waves propagating in an isotropic medium due to the rotation may be of the same order as the error caused by the principal component of $\delta(u_i'')$, it is not taken into account in this paper. Thus, the additional components of error $\delta(u_i'')$ in second derivative u_i'' are neglected here.

The error of $\delta(u_i'')$ in u_i'' causes the relative complex–valued error of

$$\Delta = \frac{1}{2}\frac{u_i\delta(u_i'')}{u_m u_m''} \tag{31}$$

in the phase velocity of the wavefront along the ray. In view of (26), the above error may be approximated by

$$\Delta \simeq \frac{1}{2}\frac{H^2}{\epsilon_0^2}\frac{u_i\delta(u_i'')}{u_m u_m} = \frac{1}{2}\frac{h^2}{v^2\epsilon^2}\frac{u_i\delta(u_i'')}{u_m u_m} \quad . \tag{32}$$

4.4 Distortion of monochromatic waves

The resulting relative error Δ_u (relative waveform misfit) of the monochromatic wavefield u_i, $\delta(u_i) \simeq u_i\Delta_u$, accumulated during time t along a ray of length s, is

$$\Delta_u \simeq -\mathrm{i}\frac{2\pi}{T}\int\limits_0^s \frac{\Delta}{v}\mathrm{d}s = -\mathrm{i}\frac{2\pi}{T}\int\limits_0^t \Delta\mathrm{d}t \quad . \tag{33}$$

This error accumulates with increasing time of propagation and there comes an instant of time at which interference waves cannot be evaluated correctly (Sei 1993). Thus, the relative phase–velocity error should be chosen inversely proportional to the time interval of the finite–difference calculation.

For example, if the average relative phase velocity error is 10^{-3}, the relative error of the calculated wavefield (relative waveform misfit) at time $t = 10\ T$ is about 6%, at time $t = 40\ T$ about 25%. If the average relative phase–velocity error is 10^{-2}, the relative error of the calculated wavefield (relative waveform misfit) at time $t = 8\ T$ is about 50%.

4.5 Distortion of wave packets

The relative phase–velocity error Δ increases with the K^{th} power of frequency $f = T^{-1}$, where K is the order of the finite difference scheme, $K = 2$ or $K = 4$. Then the wavefronts of the wave packet propagate along the ray with the relative velocity error of Δ approximately corresponding to the prevailing frequency, whereas the packet envelope propagates with the relative group–velocity error of

$$\Delta_{\mathrm{G}} = \Delta + f\frac{\mathrm{d}\Delta}{\mathrm{d}f} = (K+1)\Delta \quad . \tag{34}$$

Thus the erroneous time shift of the packet envelope, caused by the real part of the relative phase–velocity error, is $(K+1)$-times greater than the time shift of the wavefronts. This causes the phase shift of the wave packet of

$$-K\frac{2\pi}{T}\int_0^t \mathrm{Re}(\Delta)\mathrm{d}t \quad . \tag{35}$$

Similarly, the relative amplitude error of the packet envelope, caused by the imaginary part of the relative phase–velocity error, is approximately $(K+1)$-times greater than the relative error of the amplitude of the monochromatic wave of the same prevailing frequency.

5 Sources of the relative phase–velocity error

5.1 Error due to finite differences of the second order with respect to time

First, we shall study the error of the finite–difference scheme

$$u_i(\mathbf{x}, t+H) = 2u_i(\mathbf{x}, t) - u_i(\mathbf{x}, t-H) + H^2 u_i''(\mathbf{x}, t) \tag{36}$$

along the time axis.

The error of this scheme is caused by neglecting the fourth derivative u_i'''' with respect to time on the right–hand side. The error in u_i'' due to neglecting term $2\frac{H^4}{24}u_i''''$ is

$$\delta(u_i'') \simeq -\frac{H^2}{12}u_i'''' \simeq -\frac{H^2}{12}u_i\left(\frac{\epsilon_0}{H}\right)^4 = -\frac{H^{-2}}{12}u_i\epsilon_0^4 \quad . \tag{37}$$

Inserting this estimate into (32) we arrive at the relative phase–velocity error of

$$\Delta^{(0)} \simeq -\frac{1}{24}\epsilon_0^2 \tag{38}$$

corresponding to the second–order scheme (36), see equation (6) by Dablain (1986). For example, in choosing 40 time steps per one period, $H = T/40$, the relative phase velocity error is 10^{-3}, whereas for 13 time steps per one period, $H = T/13$, the relative phase velocity error is 10^{-2}. The relative group–velocity error is 3 times greater and, e.g., for $H = T/13$ the erroneous phase shift of wave packets at time $t = 13\ T$ is about $\pi/2$. However, this error may be eliminated by calculating fourth (or even higher) wavefield derivatives with respect to time by a recursive application of a spatial finite–difference scheme (Igel, Mora and Riollet, 1995). This error may, to some extent, also be eliminated by means of time and phase corrections applied to the Gabor transforms of synthetic seismograms.

5.2 Error due to finite differences in space

The error of (12) is

$$\delta(u_i'') = \delta(\rho^{-1}C_{ijkl})U_{klj} + \rho^{-1}C_{ijkl}\delta(U_{klj}) + \rho^{-1}C_{ijklj}\delta(U_{kl}) + \delta(\rho^{-1}C_{ijklj})U_{kl} \ . \quad (39)$$

The values ρ^{-1} and C_{ijkl} of material parameters are assumed to be exact, $\delta(\rho^{-1}) = 0$ and $\delta(C_{ijkl}) = 0$, and the wavefield derivatives may be approximated by (27). Then

$$\delta(u_i'') = \rho^{-1}C_{ijkl}\delta(U_{klj}) + \rho^{-1}C_{ijklj}\delta(U_{kl}) + \rho^{-1}\delta(C_{ijklj})U_k\epsilon_l h^{-1} \quad . \qquad (40)$$

Inserting this into (32), we arrive at

$$\Delta - \Delta^{(0)} \simeq \frac{1}{2}\frac{1}{\rho v^2\epsilon^2}\frac{U_i}{U_m U_m}\left[C_{ijkl}\delta(U_{klj})h^2 + C_{ijklj}\delta(U_{kl})h^2 + \delta(C_{ijklj})U_k\epsilon_l h\right] \ . \quad (41)$$

Assuming that the errors $\delta(U_{ij})$ and $\delta(U_{ijk})$ of the first and second wavefield derivatives may be expressed in terms of the corresponding relative errors Δ_j and Δ_{jk} of the finite–difference scheme,

$$\delta(U_{ij}) = U_{ij}\Delta_j \simeq U_i\epsilon_j h^{-1}\Delta_j \quad , \qquad (42)$$

$$\delta(U_{ijk}) = U_{ijk}\Delta_{jk} \simeq U_i\epsilon_j\epsilon_k h^{-2}\Delta_{jk} \quad , \qquad (43)$$

where no summation is taken over indices j and k, we arrive at

$$\Delta - \Delta^{(0)} \simeq \frac{1}{2}\frac{1}{\rho v^2\epsilon^2}\frac{U_i}{U_m U_m} \times \left[\sum_{l=1}^{3}\sum_{j=1}^{3} C_{ijkl}U_k\epsilon_l\epsilon_j\Delta_{lj} + \sum_{l=1}^{3} C_{ijklj}U_k\epsilon_l h\Delta_l + \delta(C_{ijklj})U_k\epsilon_l h\right] \ . \quad (44)$$

The total relative phase–velocity error may then be expressed in the form of

$$\Delta = \Delta^{(0)} + \Delta^{(1)} + \Delta^{(2)} + \Delta^{(3)} + \Delta^{(4)} \quad , \qquad (45)$$

with

$$\Delta^{(1)} \simeq \frac{1}{2}\frac{1}{\rho v^2\epsilon^2}e_i e_k \sum_{l=1}^{3}\sum_{j=1}^{3} C_{ijkl}\epsilon_l\epsilon_j\Delta_{lj} \qquad (46)$$

being the relative phase–velocity error caused by the inaccurate second partial wavefield derivatives,

$$\Delta^{(2)} \simeq \frac{1}{2}\frac{h}{\rho v^2\epsilon^2}e_i e_k \sum_{l=1}^{3} C_{ijklj}\epsilon_l\Delta_l \qquad (47)$$

being the relative phase–velocity error caused by the inaccurate first partial wavefield derivatives, and

$$\Delta^{(3)} \simeq \frac{1}{2}\frac{h}{\rho v^2\epsilon^2}e_i e_k \delta(C_{ijklj})\epsilon_l \qquad (48)$$

being the relative phase–velocity error caused by the inaccurate first partial derivatives of the elastic parameters. Error $\Delta^{(4)}$ caused by the inaccurate values of the elastic parameters due to the interpolation between gridpoints applies especially to the staggered grids and is zero for the centred point finite–difference schemes, $\Delta^{(4)} = 0$.

These contributions $\Delta^{(1)}$, $\Delta^{(2)}$, $\Delta^{(3)}$, and $\Delta^{(4)}$ (if applicable) to the whole relative phase–velocity error Δ will be estimated in the next sections.

6 Partial finite–difference schemes

As mentioned above, the only partial wavefield derivatives at $\mathbf{x}$, appearing in equation (12) and thus influencing the time development of the wavefield, are the first and second derivatives $U_{i[j]}$ and $U_{i[jk]}$.

Thus, we shall first study the relative errors Δ_j of $U_{i[j]}$, and Δ_{jk} of $U_{i[jk]}$, in approximation (21). Since the approximations of the individual partial derivatives in (21) are, to some extent, independent for most symmetric finite–difference schemes, we may decompose the finite–difference schemes into several partial schemes for individual partial derivatives, and to estimate the relative error of each partial derivative independently. These results will then be used to estimate the relative phase–velocity errors of the waves of particular polarizations (P, S_1, and S_2) in several finite–difference schemes.

The centred finite–difference schemes with all wavefield values and material parameters specified or calculated at the gridpoints are composed of finite–difference schemes centred at gridpoints. On the other hand, the staggered schemes are, as a rule, composed of 1-D half–interval partial finite–difference schemes for the first partial derivatives.

For 1-D partial finite–difference schemes of even orders from 2 to 10 centred at gridpoints and for their accuracy refer, e.g., to Bickley (1941). For 1-D half–interval partial finite–difference schemes of even orders from 2 to 10 refer, e.g., to Keller and Pereyra (1978). For a general algorithm to generate arbitrary 1-D partial finite–difference schemes refer to Fornberg (1988). For the 2-D partial finite–difference scheme of the 2^{nd} order centred at a gridpoint refer, e.g., to Abramowitz and Stegun (1964).

6.1 Partial scheme, 1-D, 3-point, 2^{nd} order (Fig. 1)

Figure 1.

Wavefield grid values (arguments):

$$u_{i(n_1,0,0)},\ n_1 = -1, 0, +1 \quad . \tag{49}$$

Determined Taylor–expansion coefficients:

$$U_i, U_{i[1]}, U_{i[11]} \quad . \tag{50}$$

Most important neglected Taylor–expansion coefficients:

$$U_{i[111]}, U_{i[1111]} \quad . \tag{51}$$

Finite–difference equation for the first partial derivative inside a geological block (*1 floating–point operation* per $2hU_{i[1]}$):

$$2hU_{i[1]} = u_{i(+1,0,0)} - u_{i(-1,0,0)} \quad . \tag{52}$$

Finite–difference equation for the second partial derivative inside a geological block (*3 floating–point operations* per $h^2U_{i[11]}$):

$$h^2U_{i[11]} = u_{i(+1,0,0)} + u_{i(-1,0,0)} - 2u_{i(0,0,0)} \quad . \tag{53}$$

Relative error in $hU_{i[1]} \simeq U_i\epsilon_1$ due to neglecting $h^3U_{i[111]} \simeq U_i\epsilon_1^3$ inside geological blocks:

$$\Delta_1 = \frac{1}{2}\frac{1}{\epsilon_1}\left[1+1\right]\frac{\epsilon_1^3}{6} = \frac{1}{6}\epsilon_1^2 \quad . \tag{54}$$

Relative error in $h^2U_{i[11]} \simeq U_i\epsilon_1^2$ due to neglecting $h^4U_{i[1111]} \simeq U_i\epsilon_1^4$ inside geological blocks:

$$\Delta_{11} = \frac{1}{\epsilon_1^2}\left[1+1\right]\frac{\epsilon_1^4}{24} = \frac{1}{12}\epsilon_1^2 \quad . \tag{55}$$

Analogously in the directions of the 2$^{\text{nd}}$ and 3$^{\text{rd}}$ coordinate axes,

$$\Delta_j = \frac{1}{6}\epsilon_j^2 \quad , \tag{56}$$

$$\Delta_{j=k} = \frac{1}{12}\epsilon_j^2 \quad . \tag{57}$$

Note that the replacement of the homogeneous second partial difference (53) by double application of the first partial difference (52) produces 4 times increased relative error $\Delta_{j=k}$. This is the case of the conventional methods based on the first–order systems of equations for u_i and stress σ_{ij}.

6.2 Partial scheme, 1-D, 5-point, 4$^{\text{th}}$ order (Fig. 2)

Figure 2.

Wavefield grid values (arguments):

$$u_{i(n_1,0,0)}, \; n_1 = -2,-1,0,+1,+2 \quad . \tag{58}$$

Determined Taylor–expansion coefficients:

$$U_i, U_{i[1]}, U_{i[11]}, U_{i[111]}, U_{i[1111]} \quad . \tag{59}$$

Most important neglected Taylor–expansion coefficients:

$$U_{i[11111]}, U_{i[111111]} \quad . \tag{60}$$

Finite–difference equation for the first partial derivative inside a geological block (*4 floating–point operations* per $12hU_{i[1]}$):

$$12hU_{i[1]} = 8(u_{i(+1,0,0)} - u_{i(-1,0,0)}) - (u_{i(+2,0,0)} - u_{i(-2,0,0)}) \quad . \tag{61}$$

Finite–difference equation for the second partial derivative inside a geological block (*6 floating–point operations* per $12h^2U_{i[11]}$):

$$12h^2U_{i[11]} = 16(u_{i(+1,0,0)} + u_{i(-1,0,0)}) - (u_{i(+2,0,0)} + u_{i(-2,0,0)}) - 30u_{i(0,0,0)} \quad . \tag{62}$$

Relative error in $hU_{i[1]} \simeq U_i\epsilon_1$ due to neglecting $h^5U_{i[11111]} \simeq U_i\epsilon_1^5$ inside geological blocks:

$$\Delta_1 = \frac{1}{12}\frac{1}{\epsilon_1}\left[8(1+1)-(32+32)\right]\frac{\epsilon_1^5}{120} = -\frac{1}{30}\epsilon_1^4 \quad . \tag{63}$$

Relative error in $h^2 U_{i[11]} \simeq U_i \epsilon_1^2$ due to neglecting $h^6 U_{i[111111]} \simeq U_i \epsilon_1^6$ inside geological blocks:

$$\Delta_{11} = \frac{1}{12} \frac{1}{\epsilon_1^2} \left[16(1+1) - (64+64) \right] \frac{\epsilon_1^6}{720} = -\frac{1}{90} \epsilon_1^4 \quad . \tag{64}$$

Analogously in the directions of the 2$^{\text{nd}}$ and 3$^{\text{rd}}$ coordinate axes,

$$\Delta_j = -\frac{1}{30} \epsilon_j^4 \quad , \tag{65}$$

$$\Delta_{j=k} = -\frac{1}{90} \epsilon_j^4 \quad . \tag{66}$$

Note that the replacement of the homogeneous second partial difference (62) by double application of the first partial difference (61) produces 6 times increased relative error $\Delta_{j=k}$. This is the case of the conventional methods based on the first–order systems of equations for u_i and stress σ_{ij}.

6.3 Partial scheme, 2-D, 4-point, 2$^{\text{nd}}$ order (Fig. 3)

This scheme for the mixed second derivatives is equivalent to the double application of the partial 1-D 3-point scheme (52) for the first derivatives.

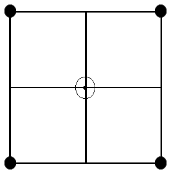

Figure 3.

Wavefield grid values (arguments):

$$u_{i(\pm 1, \pm 1, 0)} \quad . \tag{67}$$

Determined Taylor–expansion coefficients in addition to 1-D partial schemes:

$$U_{i[12]}, U_{i[112]}, U_{i[122]}, U_{i[1122]} \quad . \tag{68}$$

Most important neglected Taylor–expansion coefficients in addition to 1-D partial schemes:

$$U_{i[1112]}, U_{i[1222]}, U_{i[11112]}, U_{i[11122]}, U_{i[11222]}, U_{i[12222]} \quad . \tag{69}$$

Finite–difference equation for the second partial derivative inside a geological block:

$$4h^2 U_{i12} = 2h^2 U_{i[12]} = u_{i(+1,+1,0)} - u_{i(-1,+1,0)} - u_{i(+1,-1,0)} + u_{i(-1,-1,0)} \quad . \tag{70}$$

This could take 3 floating–point operations per $4h^2 U_{i12}$. However, if the first derivatives resulting from (52) are stored, the evaluation of (70) by means of the second application of (52) takes only *1 additional floating–point operation* per $4h^2 U_{i12}$.
Relative error in $h^2 U_{i[12]} \simeq 2U_i \epsilon_1 \epsilon_2$ due to neglecting $h^4 U_{i[1112]} \simeq 4U_i \epsilon_1^3 \epsilon_2$ and $h^4 U_{i[1222]} \simeq 4U_i \epsilon_1 \epsilon_2^3$ inside geological blocks:

$$\Delta_{12} = \frac{1}{2} \frac{1}{2\epsilon_1 \epsilon_2} \left[1+1+1+1 \right] \left(\frac{4\epsilon_1^3 \epsilon_2}{24} + \frac{4\epsilon_1 \epsilon_2^3}{24} \right) = \frac{1}{6} (\epsilon_1^2 + \epsilon_2^2) \quad . \tag{71}$$

Analogously in the $x_1 x_3$ and $x_2 x_3$ planes,

$$\Delta_{j \neq k} = \frac{1}{6} (\epsilon_j^2 + \epsilon_k^2) \quad , \tag{72}$$

which, of course, corresponds to errors (56) of the double application of (52) in directions j and k.

6.4 Partial scheme, 2-D, 8-point, 4th order (Fig. 4)

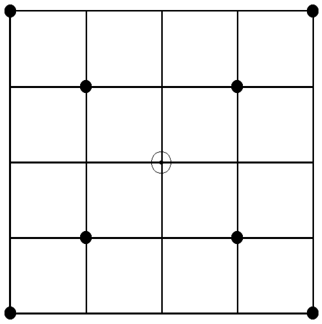

Figure 4.

Wavefield grid values (arguments):

$$u_{i(\pm1,\pm1,0)},\ u_{i(\pm2,\pm2,0)} \quad . \tag{73}$$

Determined Taylor–expansion coefficients in addition to 1-D 5-point partial schemes:

$$\begin{gathered} U_{i[12]}, U_{i[112]}, U_{i[122]}, U_{i[1122]}, U_{i[1112]} + U_{i[1222]}, \\ U_{i[11112]} + U_{i[11222]}, U_{i[11122]} + U_{i[12222]}, \\ U_{i[111111]} + U_{i[111122]} + U_{i[112222]} + U_{i[222222]} \quad . \end{gathered} \tag{74}$$

Most important neglected Taylor–expansion coefficients in addition to 1-D 5-point partial schemes:

$$\begin{gathered} U_{i[1112]} - U_{i[1222]}, U_{i[11112]} - U_{i[11222]}, U_{i[11122]} - U_{i[12222]}, \\ U_{i[111111]} - U_{i[111122]}, U_{i[111111]} - U_{i[112222]}, U_{i[111111]} - U_{i[222222]}, \\ U_{i[111112]}, U_{i[111222]}, U_{i[122222]} \quad . \end{gathered} \tag{75}$$

Finite–difference equation for the second partial derivative inside a geological block (*8 floating–point operations* per $48h^2U_{i12}$):

$$\begin{aligned} 48h^2U_{i12} = 24h^2U_{i[12]} = {} & 16(u_{i(+1,+1,0)} - u_{i(-1,+1,0)} - u_{i(+1,-1,0)} + u_{i(-1,-1,0)}) \\ & -(u_{i(+2,+2,0)} - u_{i(-2,+2,0)} - u_{i(+2,-2,0)} + u_{i(-2,-2,0)}) \ . \end{aligned} \tag{76}$$

Relative error in $h^2U_{i[12]} \simeq 2U_i\epsilon_1\epsilon_2$ due to neglecting $h^6U_{i[111112]} \simeq 6U_i\epsilon_1^5\epsilon_2$, $h^6U_{i[111222]} \simeq 20U_i\epsilon_1^3\epsilon_2^3$, and $h^6U_{i[122222]} \simeq 6U_i\epsilon_1\epsilon_2^5$ inside geological blocks:

$$\begin{aligned} \Delta_{12} &= \frac{1}{24}\frac{1}{2\epsilon_1\epsilon_2}[16(1+1+1+1) - (64+64+64+64)]\left(\frac{6\epsilon_1^5\epsilon_2^1}{720} + \frac{20\epsilon_1^3\epsilon_2^3}{720} + \frac{6\epsilon_1\epsilon_2^5}{720}\right) \\ &= -\frac{1}{180}\left(6\epsilon_1^4 + 20\epsilon_1^2\epsilon_2^2 + 6\epsilon_2^4\right) \ . \end{aligned} \tag{77}$$

Analogously in the x_1x_3 and x_2x_3 planes,

$$\Delta_{j\neq k} = -\frac{1}{180}(6\epsilon_j^4 + 20\epsilon_j^2\epsilon_k^2 + 6\epsilon_k^4) \quad . \tag{78}$$

6.5 Partial scheme, 2-D, 12-point, 4$^{\text{th}}$ order (Fig. 5)

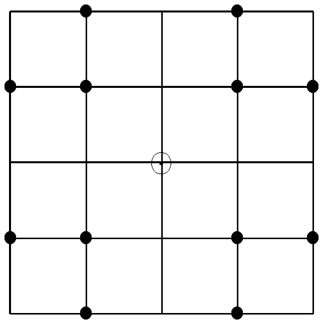

Figure 5.

Wavefield grid values (arguments):

$$u_{i(\pm1,\pm1,0)},\ u_{i(\pm2,\pm1,0)},\ u_{i(\pm1,\pm2,0)} \quad . \tag{79}$$

Determined Taylor–expansion coefficients in addition to 1-D 5-point partial schemes:

$$U_{i[12]}, U_{i[112]}, U_{i[122]}, U_{i[1112]}, U_{i[1122]}, U_{i[1222]},$$

$$U_{i[11112]}, U_{i[11122]}, U_{i[11222]}, U_{i[12222]}, U_{i[111122]}, U_{i[112222]} \quad . \tag{80}$$

Most important neglected Taylor–expansion coefficients in addition to 1-D 5-point partial schemes:

$$U_{i[111112]}, U_{i[111222]}, U_{i[122222]},$$

$$U_{i[1111112]}, U_{i[1111122]}, U_{i[1111222]}, U_{i[1112222]}, U_{i[1122222]}, U_{i[1222222]} \quad . \tag{81}$$

Finite–difference equation for the second partial derivative inside a geological block (*12 floating–point operations* per $24h^2U_{i12}$):

$$\begin{aligned} 24h^2U_{i12} = 12h^2U_{i[12]} = 10(&u_{i(+1,+1,0)} - u_{i(-1,+1,0)} - u_{i(+1,-1,0)} + u_{i(-1,-1,0)}) \\ -(&u_{i(+2,+1,0)} - u_{i(-2,+1,0)} - u_{i(+2,-1,0)} + u_{i(-2,-1,0)}) \\ -(&u_{i(+1,+2,0)} - u_{i(-1,+2,0)} - u_{i(+1,-2,0)} + u_{i(-1,-2,0)}) \ . \end{aligned} \tag{82}$$

Relative error in $h^2U_{i[12]} \simeq 2U_i\epsilon_1\epsilon_2$ due to neglecting $h^6U_{i[111112]} \simeq 6U_i\epsilon_1^5\epsilon_2$, $h^6U_{i[111222]} \simeq 20U_i\epsilon_1^3\epsilon_2^3$, and $h^6U_{i[122222]} \simeq 6U_i\epsilon_1\epsilon_2^5$ inside geological blocks:

$$\begin{aligned} \Delta_{12} = \frac{1}{12}\frac{1}{2\epsilon_1\epsilon_2}\Bigg[&(10\times4-4\times32-4\times2)\times\frac{6\epsilon_1^5\epsilon_2}{720}+(10\times4-4\times8-4\times8)\times\frac{20\epsilon_1^3\epsilon_2^3}{720} \\ &+(10\times4-4\times2-4\times32)\times\frac{6\epsilon_1\epsilon_2^5}{720}\Bigg] = -\frac{1}{180}(6\epsilon_1^4+5\epsilon_1^2\epsilon_2^2+6\epsilon_2^4) \ . \end{aligned} \tag{83}$$

Analogously in the x_1x_3 and x_2x_3 planes,

$$\Delta_{j\neq k} = -\frac{1}{180}(6\epsilon_j^4+5\epsilon_j^2\epsilon_k^2+6\epsilon_k^4) \quad . \tag{84}$$

6.6 Partial scheme, 2-D, 16-point, 4$^{\text{th}}$ order (Fig. 6)

This scheme for the mixed second derivatives is equivalent to the double application of the partial 1-D 5-point scheme (61) for the first derivatives.

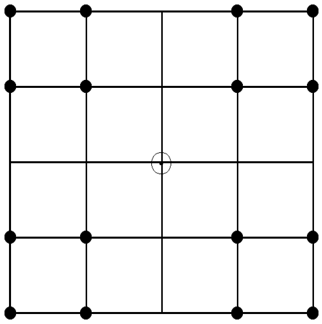

Figure 6.

Wavefield grid values (arguments):

$$u_{i(\pm1,\pm1,0)},\ u_{i(\pm2,\pm1,0)},\ u_{i(\pm1,\pm2,0)},\ u_{i(\pm2,\pm2,0)} \quad . \tag{85}$$

Determined Taylor–expansion coefficients in addition to 1-D 5-point partial schemes:

$$U_{i[12]}, U_{i[112]}, U_{i[122]}, U_{i[1112]}, U_{i[1122]}, U_{i[1222]}, U_{i[11112]}, U_{i[11122]}, U_{i[11222]}, U_{i[12222]},$$
$$U_{i[111122]}, U_{i[111222]}, U_{i[112222]}, U_{i[1111222]}, U_{i[1112222]}, U_{i[11112222]} \quad . \tag{86}$$

Most important neglected Taylor–expansion coefficients in addition to 1-D 5-point partial schemes:

$$U_{i[111112]}, U_{i[122222]}, U_{i[1111112]}, U_{i[1111122]}, U_{i[1122222]}, U_{i[1222222]} \quad . \tag{87}$$

Finite–difference equation for the second partial derivative inside a geological block:

$$\begin{aligned} 18h^2U_{i12} = 9h^2U_{i[12]} = {} & 8(u_{i(+1,+1,0)} - u_{i(-1,+1,0)} - u_{i(+1,-1,0)} + u_{i(-1,-1,0)}) \\ & -(u_{i(+2,+1,0)} - u_{i(-2,+1,0)} - u_{i(+2,-1,0)} + u_{i(-2,-1,0)}) \\ & -(u_{i(+1,+2,0)} - u_{i(-1,+2,0)} - u_{i(+1,-2,0)} + u_{i(-1,-2,0)}) \\ & +\tfrac{1}{8}(u_{i(+2,+2,0)} - u_{i(-2,+2,0)} - u_{i(+2,-2,0)} + u_{i(-2,-2,0)}) \ . \end{aligned} \tag{88}$$

This could take 17 floating–point operations per $18h^2U_{i12}$. However, if the first derivatives resulting from (61) are stored, the evaluation of (88) by means of the second application of (61) takes only *4 additional floating–point operations* per $144h^2U_{i12}$.
Relative error in $h^2U_{i[12]} \simeq 2U_i\epsilon_1\epsilon_2$ due to neglecting $h^6U_{i[111112]} \simeq 6U_i\epsilon_1^5\epsilon_2$, and $h^6U_{i[122222]} \simeq 6U_i\epsilon_1\epsilon_2^5$ inside geological blocks:

$$\begin{aligned} \Delta_{12} = \frac{1}{9}\frac{1}{2\epsilon_1\epsilon_2}\Bigg[& (8\times4 - 4\times32 - 4\times2 + \frac{1}{8}\times4\times64)\times\frac{6\epsilon_1^5\epsilon_2}{720} \\ & +(8\times4 - 4\times2 - 4\times32 + \frac{1}{8}\times4\times64)\times\frac{6\epsilon_1\epsilon_2^5}{720}\Bigg] = -\frac{1}{180}(6\epsilon_1^4 + 6\epsilon_2^4) \ . \end{aligned} \tag{89}$$

Analogously in the x_1x_3 and x_2x_3 planes,

$$\Delta_{j\neq k} = -\frac{1}{180}(6\epsilon_j^4 + 6\epsilon_k^4) \quad , \tag{90}$$

which, of course, corresponds to errors (65) of the double application of (61) in directions j and k.

6.7 Partial scheme, 1-D, half–interval 2-point, 2$^{\mathrm{nd}}$ order (Fig. 7)

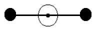

Figure 7.

Wavefield grid values (arguments):

$$u_{i(n_1,0,0)},\ n_1 = -\tfrac{1}{2}, +\tfrac{1}{2} \quad . \tag{91}$$

Determined Taylor–expansion coefficients:

$$U_i, U_{i[1]} \quad . \tag{92}$$

Most important neglected Taylor–expansion coefficients:

$$U_{i[11]}, U_{i[111]} \quad . \tag{93}$$

Finite–difference equation for the first partial derivative inside a geological block (*1 floating–point operation* per $hU_{i[1]}$):

$$hU_{i[1]} = u_{i(+\frac{1}{2},0,0)} - u_{i(-\frac{1}{2},0,0)} \quad . \tag{94}$$

This half–interval partial scheme is, as a rule, used to compose second–order staggered schemes. There is no reason to evaluate the half–interval second partial derivative here. Relative error in $hU_{i[1]} \simeq U_i\epsilon_1$ due to neglecting $h^3U_{i[111]} \simeq U_i\epsilon_1^3$ inside geological blocks is

$$\Delta_1 = \frac{1}{\epsilon_1}\left[\frac{1}{8} + \frac{1}{8}\right]\frac{\epsilon_1^3}{6} = \frac{1}{24}\epsilon_1^2 \quad . \tag{95}$$

Analogously in the directions of the 2$^{\mathrm{nd}}$ and 3$^{\mathrm{rd}}$ coordinate axes,

$$\Delta_j = \frac{1}{24}\epsilon_j^2 \quad . \tag{96}$$

6.8 Partial scheme, 1-D, half–interval 4-point, 4$^{\mathrm{th}}$ order (Fig. 8)

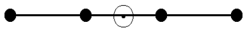

Figure 8.

Wavefield grid values (arguments):

$$u_{i(n_1,0,0)},\ n_1 = -\tfrac{3}{2}, -\tfrac{1}{2}, +\tfrac{1}{2}, +\tfrac{3}{2} \quad . \tag{97}$$

Determined Taylor–expansion coefficients:

$$U_i, U_{i[1]}, U_{i[11]}, U_{i[111]} \quad . \tag{98}$$

Most important neglected Taylor–expansion coefficients:

$$U_{i[1111]}, U_{i[11111]} \quad . \tag{99}$$

Finite–difference equation for the first partial derivative inside a geological block (*4 floating–point operations* per $24hU_{i[1]}$):

$$24hU_{i[1]} = 27(u_{i(+\frac{1}{2},0,0)} - u_{i(-\frac{1}{2},0,0)}) - (u_{i(+\frac{3}{2},0,0)} - u_{i(-\frac{3}{2},0,0)}) \quad . \tag{100}$$

This half–interval partial scheme is, as a rule, used to compose fourth–order staggered schemes. There is no reason to evaluate the half–interval second partial derivative here. Relative error in $hU_{i[1]} \simeq U_i\epsilon_1$ due to neglecting $h^5U_{i[11111]} \simeq U_i\epsilon_1^5$ inside geological blocks is

$$\Delta_1 = \frac{1}{24}\frac{1}{\epsilon_1}\left[27(\frac{1}{32} + \frac{1}{32}) - (\frac{243}{32} + \frac{243}{32})\right]\frac{\epsilon_1^5}{120} = -\frac{3}{640}\epsilon_1^4 \quad . \tag{101}$$

Analogously in the directions of the 2$^{\mathrm{nd}}$ and 3$^{\mathrm{rd}}$ coordinate axes,

$$\Delta_j = -\frac{3}{640}\epsilon_j^4 \quad . \tag{102}$$

7 Error due to the inaccurate second partial wavefield derivatives

In this section, we shall study the relative phase–velocity errors of the most important 2-D and 3-D finite–difference schemes on regular rectangular grids in smooth isotropic media.

The relative error of the phase velocity v of the wave of a particular polarization (P, S_1, or S_2), caused by the inaccurate second partial wavefield derivatives, is given by (46) and is real–valued.

In an isotropic medium, see (9), equation (46) reads

$$\begin{aligned}
\Delta^{(1)} &\simeq \frac{1}{2}\frac{\sum_{j,k}[(\lambda+\mu)e_j e_k + \mu\delta_{jk}]\epsilon_j\epsilon_k\Delta_{jk}}{\rho v^2\epsilon^2} \\
&= \frac{1}{2}\frac{\sum_{j,k}[({v_{\mathrm{P}}}^2-{v_{\mathrm{S}}}^2)e_j e_k + {v_{\mathrm{S}}}^2\delta_{jk}]\epsilon_j\epsilon_k\Delta_{jk}}{v^2\epsilon^2} \\
&= \frac{1}{2v^2}\left\{\sum_j[({v_{\mathrm{P}}}^2-{v_{\mathrm{S}}}^2)e_j^2+{v_{\mathrm{S}}}^2]\epsilon_j^2\Delta_{jj} + 2\sum_{j<k}({v_{\mathrm{P}}}^2-{v_{\mathrm{S}}}^2)e_j e_k\epsilon_j\epsilon_k\Delta_{jk}\right\}\epsilon^{-2}\,. \qquad (103)
\end{aligned}$$

In a special case of the propagation along a gridline, relative phase–velocity error (103) of the elastic waves is the same as the error of the acoustic waves,

$$\Delta^{(1)}_{\mathrm{gridline}} = \tfrac{1}{2}\Delta_{jj} \qquad (104)$$

with ϵ substituted for ϵ_j in Δ_{jj}.

Note that if $\Delta_{jk} = \Delta_j + \Delta_k$ (e.g., for staggered grids or the methods based on the first–order systems of equations for u_i and stress σ_{ij}), equation (103) simplifies to

$$\Delta^{(1)} \simeq \left\{\sum_j \epsilon_j^2\Delta_j\right\}\epsilon^{-2} \qquad (105)$$

independently of the wave polarization, as already noticed by Virieux (1986). If partial relative error Δ_j has its maximum along the gridlines in the j^{th} direction, then the maximum relative phase–velocity error is incurred along the gridlines,

$$\Delta^{(1)}_{\max} = \Delta_j \qquad (106)$$

with ϵ substituted for ϵ_j in Δ_j.

Now the relative errors corresponding to the particular finite–difference schemes have to be substituted for Δ_{jk} into (103) to arrive at the final error estimates.

7.1 2-D, 9-point, 2^{nd} order (Fig. 9)

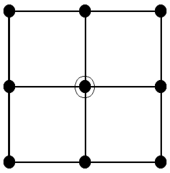

Figure 9.

This scheme, used for elastic waves in cylindrical coordinates by Alterman and Karal (1968), is composed of 1-D 3-point and 2-D 4-point partial schemes, and requires *10 floating–point operations* $\times$ *2 components* per $2hU_{I1}$, $2hU_{I2}$, h^2U_{I11}, h^2U_{I22}, h^2U_{I12}. Equation (103) with (57) and (72) reads

$$\Delta^{(1)} \simeq \frac{1}{24v^2}\left\{\sum_j[({v_\mathrm{P}}^2-{v_\mathrm{S}}^2)e_j^2+{v_\mathrm{S}}^2]\epsilon_j^4+4\sum_{j<k}({v_\mathrm{P}}^2-{v_\mathrm{S}}^2)e_je_k(\epsilon_j^3\epsilon_k+\epsilon_j\epsilon_k^3)\right\}\epsilon^{-2} . \tag{107}$$

Unfortunately, this equation does not conform with the grid dispersion curves shown by Marfurt (1984). On the other hand, for propagation along a gridline, it conforms with the grid dispersion relation for acoustic waves derived by Alford, Kelly and Boore (1974), see also equation (10) by Dablain (1986).

The maximum relative P-wave phase–velocity error for ${v_\mathrm{P}}^2 \le 3{v_\mathrm{S}}^2$ is incurred along the gridlines,

$$\Delta^{(1)}_{\max} = \frac{1}{24}\epsilon^2 \quad . \tag{108}$$

The maximum relative P-wave phase–velocity error for ${v_\mathrm{P}}^2 \ge 3{v_\mathrm{S}}^2$ is greater and is incurred along the diagonals,

$$\Delta^{(1)}_{\max} = \frac{1}{24}\left(\frac{5}{4}-\frac{3}{4}\frac{{v_\mathrm{S}}^2}{{v_\mathrm{P}}^2}\right)\epsilon^2 \quad . \tag{109}$$

The maximum relative S-wave phase–velocity error for ${v_\mathrm{P}}^2 \le 3{v_\mathrm{S}}^2$ is incurred along the gridlines,

$$\Delta^{(1)}_{\max} = \frac{1}{24}\epsilon^2 \quad . \tag{110}$$

The maximum relative S-wave phase–velocity error for ${v_\mathrm{P}}^2 \ge 3{v_\mathrm{S}}^2$ is greater and is incurred for the in–plane polarization propagating along the diagonals,

$$\Delta^{(1)}_{\max} = -\frac{1}{24}\left(\frac{3}{4}\frac{{v_\mathrm{P}}^2}{{v_\mathrm{S}}^2}-\frac{5}{4}\right)\epsilon^2 \quad . \tag{111}$$

7.2 2-D, 17-point, 4$^{\text{th}}$ order (Fig. 10)

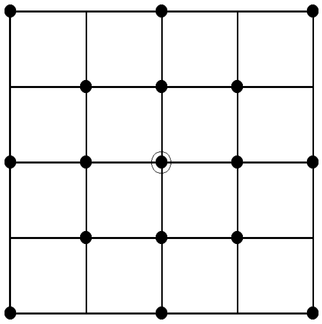

Figure 10.

This scheme is composed of 1-D 5-point and 2-D 8-point partial schemes, and requires *29 floating–point operations* $\times$ *2 components* per $12hU_{I1}$, $12hU_{I2}$, $12h^2U_{I11}$, $12h^2U_{I22}$, $12h^2U_{I12}$. Equation (103) with (66) and (78) reads

$$\Delta^{(1)} \simeq -\frac{1}{180v^2}\left\{\sum_j [({v_{\mathrm{P}}}^2 - {v_{\mathrm{S}}}^2)e_j^2 + {v_{\mathrm{S}}}^2]\epsilon_j^6 \right.$$
$$\left. + \sum_{j<k}({v_{\mathrm{P}}}^2 - {v_{\mathrm{S}}}^2)e_je_k(6\epsilon_j^5\epsilon_k + 20\epsilon_j^3\epsilon_k^3 + 6\epsilon_j\epsilon_k^5)\right\}\epsilon^{-2} \ . \tag{112}$$

The maximum relative P-wave phase–velocity error is incurred along the diagonals,

$$\Delta^{(1)}_{\max} = -\frac{1}{180}\left(\frac{17}{8} - \frac{15}{8}\frac{{v_{\mathrm{S}}}^2}{{v_{\mathrm{P}}}^2}\right)\epsilon^4 \quad . \tag{113}$$

For example, the value of (113) for ${v_{\mathrm{P}}}^2 = 3{v_{\mathrm{S}}}^2$ is

$$\Delta^{(1)}_{\max} = -\frac{1}{180}\frac{3}{2}\epsilon^4 \quad . \tag{114}$$

The maximum relative S-wave phase–velocity error is incurred for the in–plane polarization propagating along the diagonals,

$$\Delta^{(1)}_{\max} = \frac{1}{180}\left(\frac{15}{8}\frac{{v_{\mathrm{P}}}^2}{{v_{\mathrm{S}}}^2} - \frac{17}{8}\right)\epsilon^4 \quad . \tag{115}$$

For example, the value of (115) for ${v_{\mathrm{P}}}^2 = 3{v_{\mathrm{S}}}^2$ is

$$\Delta^{(1)}_{\max} = \frac{1}{180}\frac{7}{2}\epsilon^4 \quad . \tag{116}$$

7.3 2-D, 21-point, 4$^{\text{th}}$ order (Fig. 11)

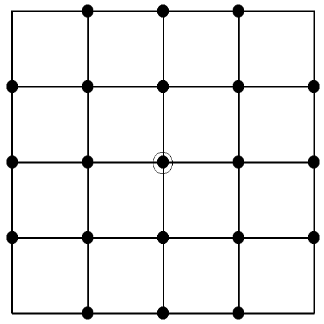

Figure 11.

This scheme is composed of 1-D 5-point and 2-D 12-point partial schemes, and requires *33 floating–point operations × 2 components* per $12hU_{I1}$, $12hU_{I2}$, $12h^2U_{I11}$, $12h^2U_{I22}$, $12h^2U_{I12}$. Equation (103) with (66) and (84) reads

$$\Delta^{(1)} \simeq -\frac{1}{180v^2}\left\{\sum_j [({v_{\mathrm{P}}}^2 - {v_{\mathrm{S}}}^2)e_j^2 + {v_{\mathrm{S}}}^2]\epsilon_j^6 + \sum_{j<k}({v_{\mathrm{P}}}^2 - {v_{\mathrm{S}}}^2)e_j e_k(6\epsilon_j^5\epsilon_k + 5\epsilon_j^3\epsilon_k^3 + 6\epsilon_j\epsilon_k^5)\right\}\epsilon^{-2} \ . \quad (117)$$

The maximum relative P-wave phase–velocity error for ${v_{\mathrm{P}}}^2 \le \frac{5}{2}{v_{\mathrm{S}}}^2$ is incurred along the gridlines,

$$\Delta^{(1)}_{\max} = -\frac{1}{180}\epsilon^4 \quad . \quad (118)$$

The maximum relative P-wave phase–velocity error for ${v_{\mathrm{P}}}^2 > \frac{5}{2}{v_{\mathrm{S}}}^2$ is greater and is incurred in the direction of unit vector $(\vartheta_1, \vartheta_2) = (\cos\alpha, \sin\alpha)$ satisfying equation

$$(\cos\alpha)^2(\sin\alpha)^2 = \frac{1}{5}\frac{{v_{\mathrm{P}}}^2 - \frac{5}{2}{v_{\mathrm{S}}}^2}{{v_{\mathrm{P}}}^2 - {v_{\mathrm{S}}}^2} \quad , \quad (119)$$

and is equal to

$$\Delta^{(1)}_{\max} = -\frac{1}{180}\left[1 + \frac{1}{5}\frac{({v_{\mathrm{P}}}^2 - \frac{5}{2}{v_{\mathrm{S}}}^2)^2}{{v_{\mathrm{P}}}^2({v_{\mathrm{P}}}^2 - {v_{\mathrm{S}}}^2)}\right]\epsilon^4 \quad . \quad (120)$$

For example, the value of (120) for ${v_{\mathrm{P}}}^2 = 3{v_{\mathrm{S}}}^2$ is

$$\Delta^{(1)}_{\max} = -\frac{1}{180}\frac{121}{120}\epsilon^4 \quad . \quad (121)$$

The maximum relative S-wave phase–velocity error for ${v_{\mathrm{P}}}^2 \le \frac{7}{3}{v_{\mathrm{S}}}^2$ is incurred along the gridlines,

$$\Delta^{(1)}_{\max} = -\frac{1}{180}\epsilon^4 \quad . \quad (122)$$

The maximum relative S-wave phase–velocity error for ${v_{\mathrm{P}}}^2 > \frac{7}{3}{v_{\mathrm{S}}}^2$ is greater and is incurred for the in–plane polarization propagating along the diagonals,

$$\Delta^{(1)}_{\max} = \frac{1}{180}\left(\frac{15}{16}\frac{{v_{\mathrm{P}}}^2}{{v_{\mathrm{S}}}^2} - \frac{19}{16}\right)\epsilon^4 \quad . \quad (123)$$

For example, the value of (123) for ${v_{\mathrm{P}}}^2 = 3{v_{\mathrm{S}}}^2$ is

$$\Delta^{(1)}_{\max} = \frac{1}{180}\frac{13}{8}\epsilon^4 \quad . \quad (124)$$

7.4 2-D, 25-point, 4^{th} order (Fig. 12)

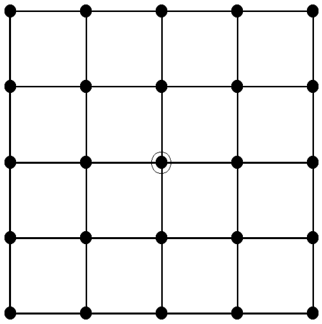

Figure 12.

This scheme is composed of 1-D 5-point and 2-D 16-point partial schemes, and requires *25 floating-point operations* $\times$ *2 components* per $12hU_{I1}$, $12hU_{I2}$, $12h^2U_{I11}$, $12h^2U_{I22}$, $12h^2U_{I12}$. Equation (103) with (66) and (90) reads

$$\Delta^{(1)} \simeq -\frac{1}{180v^2}\left\{\sum_j [({v_{\rm P}}^2 - {v_{\rm S}}^2)e_j^2 + {v_{\rm S}}^2]\epsilon_j^6 \right.$$
$$\left. + \sum_{j<k}({v_{\rm P}}^2 - {v_{\rm S}}^2)e_j e_k(6\epsilon_j^5\epsilon_k + 6\epsilon_j\epsilon_k^5)\right\}\epsilon^{-2} \quad . \qquad (125)$$

For the propagation along a gridline, equations (112), (117) and (125) give, of course, the same relative phase–velocity error, conformal with the grid dispersion relation for acoustic waves published by Alford, Kelly and Boore (1974).

The maximum relative P-wave phase–velocity error for ${v_{\rm P}}^2 \le \frac{5}{2}{v_{\rm S}}^2$ is incurred along the gridlines,

$$\Delta^{(1)}_{\max} = -\frac{1}{180}\epsilon^4 \quad . \qquad (126)$$

The maximum relative P-wave phase–velocity error for ${v_{\rm P}}^2 > \frac{5}{2}{v_{\rm S}}^2$ is greater and is incurred in the direction of unit vector $(\vartheta_1, \vartheta_2) = (\cos\alpha, \sin\alpha)$ satisfying equation

$$(\cos\alpha)^2(\sin\alpha)^2 = \frac{1}{10}\frac{{v_{\rm P}}^2 - \frac{5}{2}{v_{\rm S}}^2}{{v_{\rm P}}^2 - {v_{\rm S}}^2} \quad , \qquad (127)$$

and is equal to

$$\Delta^{(1)}_{\max} = -\frac{1}{180}\left[1 + \frac{1}{10}\frac{({v_{\rm P}}^2 - \frac{5}{2}{v_{\rm S}}^2)^2}{{v_{\rm P}}^2({v_{\rm P}}^2 - {v_{\rm S}}^2)}\right]\epsilon^4 \quad . \qquad (128)$$

For example, the value of (128) for ${v_{\rm P}}^2 = 3{v_{\rm S}}^2$ is

$$\Delta^{(1)}_{\max} = -\frac{1}{180}\frac{241}{240}\epsilon^4 \quad . \qquad (129)$$

The maximum relative S-wave phase–velocity error for ${v_{\rm P}}^2 \le 3{v_{\rm S}}^2$ is incurred along the gridlines,

$$\Delta^{(1)}_{\max} = -\frac{1}{180}\epsilon^4 \quad . \qquad (130)$$

The maximum relative S-wave phase–velocity error for $v_P{}^2 > 3v_S{}^2$ is greater and is incurred for the in–plane polarization propagating along the diagonals,

$$\Delta^{(1)}_{\max} = \frac{1}{180}\left(\frac{5}{8}\frac{v_P{}^2}{v_S{}^2} - \frac{7}{8}\right)\epsilon^4 \quad . \tag{131}$$

Thus, in an isotropic medium, this scheme is both computationally faster and more accurate, for both P waves and S waves, than the preceding 17-point and 21-point schemes. The disadvantage of this scheme is that the first wavefield derivatives have to be evaluated two grid intervals ahead and kept in the memory in order to retain the computational speed.

7.5 3-D, 19-point, 2nd order (Fig. 13)

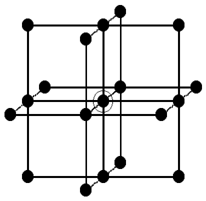

Figure 13.

This scheme is composed of 1-D 3-point and 2-D 4-point partial schemes. In view of (14), we see that not all 3 mixed second derivatives of all 3 wavefield components are needed. It is sufficient to calculate only

$$\frac{\partial}{\partial x^1}(u_{2,2}+u_{3,3}) \ , \quad \frac{\partial}{\partial x^2}(u_{1,1}+u_{3,3}) \ , \quad \frac{\partial}{\partial x^3}(u_{1,1}+u_{2,2}) \tag{132}$$

by means of the second application of (52). Costs may thus be reduced even to *15 floating–point operations* $\times$ *3 components* per $2hU_{i1}$, $2hU_{i2}$, $2hU_{i3}$, h^2U_{i11}, h^2U_{i22}, h^2U_{i33}, $h^2\sum_{j\neq i}U_{jji}$.

The accuracy is identical to the *2-D, 9-point, 2nd order* scheme, see (107) to (111).

7.6 3-D, 37-point, 4th order (Fig. 14)

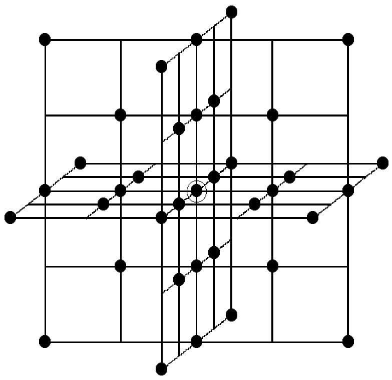

Figure 14.

This scheme is composed of 1-D 5-point and 2-D 8-point partial schemes, and requires *48 floating–point operations* $\times$ *3 components.*

The accuracy is identical to the *2-D, 17-point, 4th order* scheme, see (112) to (116).

7.7 3-D, 49-point, 4^{th} order (Fig. 15)

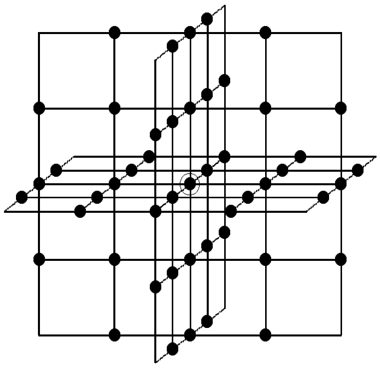

Figure 15.

This scheme is composed of 1-D 5-point and 2-D 12-point partial schemes, and requires *56 floating-point operations* $\times$ *3 components* per $12hU_{i1}$, $12hU_{i2}$, $12hU_{i3}$, $12h^2U_{i11}$, $12h^2U_{i22}$, $12h^2U_{i33}$, $12h^2\sum_{j\neq i}U_{jji}$.

The accuracy is identical to the *2-D, 21-point, 4^{th} order* scheme, see (117) to (124).

7.8 3-D, 61-point, 4^{th} order (Fig. 16)

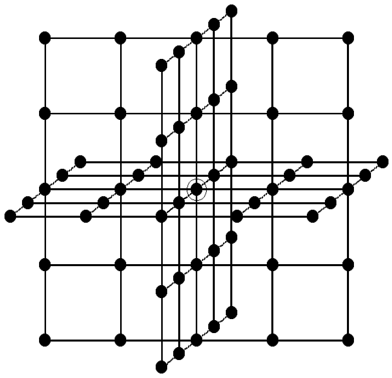

Figure 16.

This scheme is composed of 1-D 5-point and 2-D 16-point partial schemes. In view of (14), we see that not all 3 mixed second derivatives of all 3 wavefield components are needed. It is sufficient to calculate only

$$\frac{\partial}{\partial x^1}(u_{2,2}+u_{3,3}) \ , \quad \frac{\partial}{\partial x^2}(u_{3,3}+u_{1,1}) \ , \quad \frac{\partial}{\partial x^3}(u_{1,1}+u_{2,2}) \qquad (133)$$

by means of the second application of (61). Costs may thus be reduced even to *36 floating-point operations* $\times$ *3 components* per $12hU_{i1}$, $12hU_{i2}$, $12hU_{i3}$, $12h^2U_{i11}$, $12h^2U_{i22}$, $12h^2U_{i33}$, $12h^2\sum_{j\neq i}U_{jji}$, provided that $U_{22}+U_{33}$, $U_{33}+U_{11}$, and $U_{11}+U_{22}$ at surrounding gridpoints are temporarily stored in the memory.

The accuracy is identical to the *2-D, 25-point, 4^{th} order* scheme, see (125) to (131).

7.9 Staggered finite–difference schemes

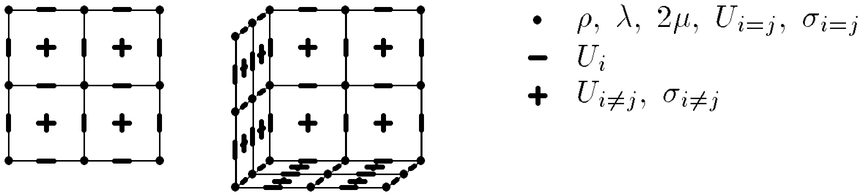

Figure 17.

The staggered schemes according to Madariaga (1976), Virieux and Madariaga (1982), Virieux (1986), and Levander (1988) are composed of 1-D half–interval partial schemes. Since accuracy of the double application of first finite differences of the 2^{nd} order in time, once for the stress and once for the wavefield, is the same as the accuracy of the second finite differences (36), we will follow Igel, Mora and Rodrigues (1991) and Sei (1993) in using equations (8) and (11) at a time instant and equation (36) with respect to time.

The components of the wavefield vector are discretized half way between gridpoints along the corresponding gridlines, their partial derivatives U_{ij} and stress components σ_{ij} for $i = j$ at the gridpoints, and for $i \neq j$ at the centres of the square faces formed by gridlines parallel with the i^{th} and j^{th} axes (Fig. 17). Material parameters are assumed to be specified at gridpoints (i.e., intersections of the gridlines), linearly interpolated along gridline intervals, and bilinearly interpolated within the square faces.

Inserting (9) into (8) we arrive at

$$\sigma_{i=j}(\mathbf{x}) = 2\mu(\mathbf{x})u_{i,j}(\mathbf{x}) + \lambda(\mathbf{x})\sum_k u_{k,k}(\mathbf{x}) \tag{134}$$

and

$$\sigma_{i\neq j}(\mathbf{x}) = [u_{i,j}(\mathbf{x}) + u_{j,i}(\mathbf{x})]\frac{1}{8}\sum_{\pm\pm} 2\mu(\mathbf{x} \pm \tfrac{1}{2}\mathbf{h}_i \pm \tfrac{1}{2}\mathbf{h}_j) \quad . \tag{135}$$

Here $2\mu(\mathbf{x})$ in the centre of the square face has been replaced by its bilinear approximation from the corner gridpoints of the face. Using linear interpolation of the density between the gridpoints, equation (11) reads

$$u_i''(\mathbf{x}) = \frac{2\sum_j \sigma_{ij,j}(\mathbf{x})}{\rho(\mathbf{x}-\frac{1}{2}\mathbf{h}_i) + \rho(\mathbf{x}+\frac{1}{2}\mathbf{h}_i)} \quad . \tag{136}$$

These equations, together with (36) and the 1-D half–interval partial schemes of the corresponding order, define the staggered finite–difference method considered here.

7.10 2-D staggered, $2^{\rm nd}$ order (Fig. 18)

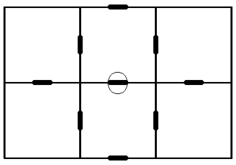

Figure 18.

This scheme is composed of 1-D 2-point half–interval partial schemes of Section 6.7. Equation (105) with (96) reads

$$\Delta^{(1)} \simeq \frac{1}{24\epsilon^2} \sum_j \epsilon_j^4 \quad . \tag{137}$$

This equation conforms with grid dispersion curves shown by Virieux (1986).

The maximum relative phase–velocity error is incurred along the gridlines,

$$\Delta^{(1)}_{\rm max} = \frac{1}{24} \epsilon^2 \quad , \tag{138}$$

see (106) with (96), and is dependent on the wave polarization through ϵ only.

7.11 2-D staggered, $4^{\rm th}$ order (Fig. 19)

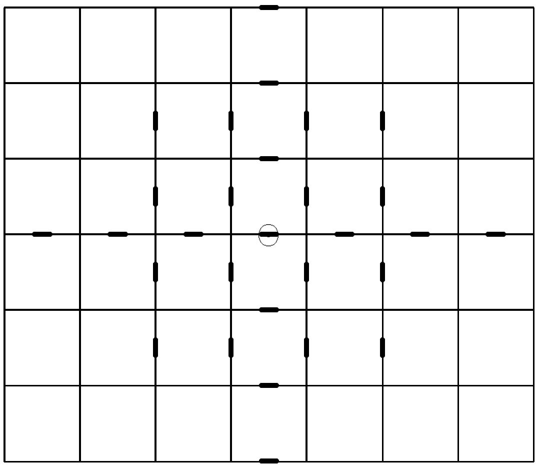

Figure 19.

This scheme is composed of 1-D 4-point half–interval partial schemes of Section 6.8. Equation (105) with (102) reads

$$\Delta^{(1)} \simeq -\frac{3}{640\epsilon^2} \sum_j \epsilon_j^6 \quad . \tag{139}$$

The maximum relative phase–velocity error is incurred along the gridlines,

$$\Delta^{(1)}_{\rm max} = -\frac{3}{640} \epsilon^4 \quad , \tag{140}$$

see (106) with (96), and is dependent on the wave polarization through ϵ only.

This staggered $4^{\rm th}$ order finite–difference scheme is thus slightly more accurate than the centred 25 point 2-D $4^{\rm th}$ order finite–difference scheme of Section 7.4, but has an extent of 6 grid intervals that would correspond to the centred finite–difference scheme of the $6^{\rm th}$ order.

7.12 3-D staggered, 2^{nd} order (Fig. 20)

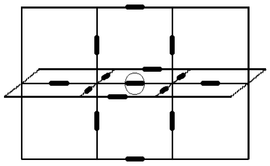

Figure 20.

This scheme is composed of 1-D 2-point half–interval partial schemes of Section 6.7.

The accuracy is identical to the 2-D staggered 2^{nd} order scheme, see (137) and (138).

7.13 3-D staggered, 4^{th} order (Fig. 21)

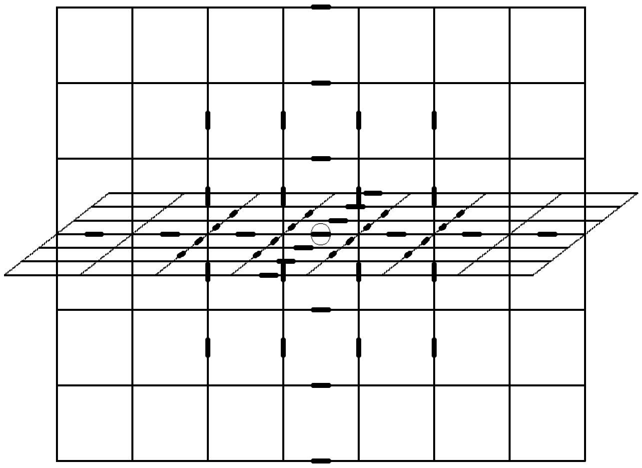

Figure 21.

This scheme is composed of 1-D 4-point half–interval partial schemes of Section 6.8.

The accuracy is identical to the 2-D staggered 4^{th} order scheme, see (139) and (140).

8 Error due to the inaccurate wavefield gradient

Inserting (56) into (47), we arrive at the estimate

$$\Delta^{(2)} \simeq \frac{1}{12} \frac{h}{\rho v^2 \epsilon^2} e_i e_k \sum_{l=1}^{3} C_{ijklj} (\epsilon_l)^3 \tag{141}$$

of the relative phase–velocity error due to the approximation of the wavefield gradient by finite differences of the second order. Similarly, inserting (65) into (47), we arrive at the estimate

$$\Delta^{(2)} \simeq -\frac{1}{60} \frac{h}{\rho v^2 \epsilon^2} e_i e_k \sum_{l=1}^{3} C_{ijklj} (\epsilon_l)^5 \tag{142}$$

of the relative phase–velocity error due to the approximation of the wavefield gradient by finite differences of the fourth order.

In an isotropic medium, the relative phase–velocity error is thus

$$\Delta^{(2)} \simeq \frac{1}{12} \frac{h}{\rho v^2 \epsilon^2} \sum_{l=1}^{3} \frac{\partial(\rho v^2)}{\partial x_l} (\epsilon_l)^3 \tag{143}$$

for the finite differences of the 2$^{\text{nd}}$ order, and

$$\Delta^{(2)} \simeq -\frac{1}{60}\frac{h}{\rho v^2 \epsilon^2}\sum_{l=1}^{3}\frac{\partial(\rho v^2)}{\partial x_l}(\epsilon_l)^5 \tag{144}$$

for the finite differences of the 4$^{\text{th}}$ order. Relative errors (143) and (144) are independent of the wave polarization.

If we denote, in an isotropic medium,

$$\frac{1}{L^{(1)}} = \max\left(\left|\frac{1}{\rho v^2}\frac{\partial(\rho v^2)}{\partial x_j}\right|,\ j=1,2,3\right) \quad , \tag{145}$$

the maximum absolute value of the imaginary relative phase–velocity error due to the inaccurate wavefield gradient is

$$\Delta^{(2)}_{\max} \simeq \frac{|\epsilon|}{12}\frac{h}{L^{(1)}} \tag{146}$$

for the finite differences of the 2$^{\text{nd}}$ order, and

$$\Delta^{(2)}_{\max} \simeq \frac{|\epsilon|^3}{60}\frac{h}{L^{(1)}} \tag{147}$$

for the finite differences of the 4$^{\text{th}}$ order. This maximum error is incurred if the wave propagates along the corresponding gridline, and should be negligible in reasonably sampled models.

Equations (141), (143) and (146) for the 2$^{\text{nd}}$ order centred finite differences are applicable also to the 2$^{\text{nd}}$ order staggered finite differences. Equations (142), (144) and (147) are in force only for the 4$^{\text{th}}$ order centred finite differences, still similar expressions for the 4$^{\text{th}}$ order staggered finite differences can be derived.

9 Error due to the inaccurate gradients of material parameters

The error of approximation (17) is

$$\delta(C_{ijklm}) \simeq \frac{h^2}{6}\frac{\partial^3 c_{ijkl}}{(\partial x_m)^3}(\mathbf{x}) \quad . \tag{148}$$

Inserting (148) into (48) we arrive at

$$\Delta^{(3)} \simeq \frac{1}{12}\frac{h^3}{\rho v^2 \epsilon^2} e_i e_k \epsilon_l \sum_{j=1}^{3}\frac{\partial^3 c_{ijkl}}{(\partial x_j)^3}(\mathbf{x}) \quad . \tag{149}$$

In an isotropic medium, the relative phase–velocity error is thus

$$\Delta^{(3)} \simeq \frac{1}{12}\frac{h^3}{\rho v^2 \epsilon^2}\sum_{j=1}^{3}\epsilon_j\frac{\partial^3(\rho v^2)}{(\partial x_j)^3} \quad . \tag{150}$$

Relative error (150) is independent of the wave polarization.

If we denote, in an isotropic medium,

$$\frac{1}{L^{(3)}} = \max\left(\left| \frac{1}{\rho v^2} \frac{\partial^3(\rho v^2)}{(\partial x_j)^3} \right| ,\ j=1,2,3 \right) \quad , \tag{151}$$

the maximum absolute value of the imaginary relative phase–velocity error due to the inaccurate gradient of the elastic parameters is

$$\Delta^{(3)}_{\max} \simeq \frac{1}{12|\epsilon|} \frac{h^3}{L^{(3)}} \quad . \tag{152}$$

Here ϵ in the denominator looks dangerously for low frequencies at first glance, but implies no problems. Relative phase–velocity error (152) causes an error of the order of $\frac{1}{12}\frac{h^2}{L^{(2)}}$, with

$$\frac{1}{L^{(2)}} = \max\left(\left| \frac{1}{\rho v^2} \frac{\partial^2(\rho v^2)}{(\partial x_j)^2} \right| ,\ j=1,2,3 \right) \quad , \tag{153}$$

in the wavefield amplitudes, independently of the wavelength. Such an error should be negligible in all reasonably sampled models, independently of the order of the finite–difference scheme used.

This error is 4 times reduced for staggered finite differences of the 2$^{\mathrm{nd}}$ order, and is even much smaller for staggered finite differences of the 4$^{\mathrm{th}}$ order.

10 Error due to the inaccurate values of material parameters

Staggered finite differences introduce another, usually also negligible, real–valued relative phase–velocity error due to the interpolation of the material parameters between the gridpoints. The bilinear and linear interpolations are explicitly expressed in equation (135) and in the denominator of equation (136), but the linear interpolation of material parameters between gridpoints, hidden in the numerator of (136), also takes place if staggered finite differences of the 2$^{\mathrm{nd}}$ order are used.

For example, maximum absolute relative phase–velocity error due to the inaccurate values of material parameters, corresponding to a wave propagating along a gridline, is (a) for P wave calculated by staggered finite differences of the 2$^{\mathrm{nd}}$ order

$$\Delta^{(4)}_{\max} \simeq \frac{1}{16} \frac{h^2}{\Lambda^{(2)}} \quad , \tag{154}$$

(b) for S wave calculated by staggered finite differences of the 2$^{\mathrm{nd}}$ order

$$\Delta^{(4)}_{\max} \lesssim \frac{1}{16} \frac{h^2}{\Lambda^{(2)}} + \frac{1}{8} \frac{h^2}{L^{(2)}} \quad , \tag{155}$$

(c) for P wave calculated by staggered finite differences of the 4$^{\mathrm{th}}$ order

$$\Delta^{(4)}_{\max} \simeq \frac{1}{16} \frac{h^2}{R^{(2)}} \quad , \tag{156}$$

(d) for S wave calculated by staggered finite differences of the 4^{th} order

$$\Delta_{\max}^{(4)} \lesssim \frac{1}{16}\frac{h^2}{\Lambda^{(2)}} + \frac{1}{16}\frac{h^2}{L^{(2)}} \quad , \tag{157}$$

with

$$\frac{1}{\Lambda^{(2)}} = \max\left(\left| \frac{1}{v^2}\frac{\partial^2(v^2)}{(\partial x_j)^2} \right| , \ j=1,2,3 \right) \tag{158}$$

and

$$\frac{1}{R^{(2)}} = \max\left(\left| \frac{1}{\rho}\frac{\partial^2 \rho}{(\partial x_j)^2} \right| , \ j=1,2,3 \right) \quad . \tag{159}$$

The maximum absolute relative phase–velocity errors in other directions will likely not differ considerably from these estimates.

11 Efficiency estimations

11.1 Centred point 2-D and 3-D schemes

Assume to use the best 4^{th} order schemes of Sections 7.4 or 7.8, and to have stored, in addition to the wavefield components in 2 time instants, also isotropic elastic parameters λ, μ, and $\frac{12h^2}{H^2}\rho$ in the computer RAM (random–access memory).

Evaluation of $12h^2U_{i1}$, $12h^2U_{i2}$, $12h^2U_{i3}$ (in 3-D), $12h^2U_{i11}$, $12h^2U_{i22}$, $12h^2U_{i33}$ (in 3-D), $12h^2\sum_{j\neq i}U_{jji}$ using the 4^{th} order schemes of Sections 7.4 or 7.8 requires *25 (in 2-D)* or *36 (in 3-D) floating-point operations per component.* For this class of even–order finite–difference schemes, the number of floating–point operations per component increases by 15 (in 2-D) or 21 (in 3-D) if the order of the scheme is increased by 2.

Evaluation of $2h\frac{\partial\lambda}{\partial x_i}(\mathbf{x})$, $2h\frac{\partial\mu}{\partial x_i}(\mathbf{x})$ using (17) requires *2 additional floating-point operations per component.*

Evaluation of $12h^2C_{ijklj}U_{kl}$ using (16) requires *8 (in 2-D)* or *10+2/3 (in 3-D) additional floating-point operations per component.*

Evaluation of $12h^2C_{ijkl}U_{klj}$ using (14) requires *5 (in 2-D)* or *6 (in 3-D) additional floating–point operations per component*, plus *1 floating–point operation* for the addition in $\lambda+\mu$.

Evaluation of $H^2u_i''(\mathbf{x})$ using (12) requires *2 additional floating-point operations per component.*

Finally, evaluation of (36) requires *3 additional floating–point operations per component.*

The total number of floating–point operations per gridpoint, required to calculate the elastic wavefield in the next time instant using the finite–difference scheme of the 4^{th} order, is thus *45×2+1=91 floating-point operations* in 2-D, or *59×3+2+1=180 floating-point operations* in 3-D.

In general, the total number of floating–point operations per gridpoint, required to calculate the elastic wavefield in the next time instant using the centred finite–difference scheme of the K^{th} order, is *31+30K/2 floating-point operations* in 2-D, or *54+63K/2 floating-point operations* in 3-D.

11.2 Staggered 2-D and 3-D schemes

Assume to use the staggered schemes of Sections 7.9 to 7.13, and to have stored, in addition to the wavefield components at "staggered" points in 2 time instants, also isotropic elastic parameters λ, 2μ, and $\frac{c^2}{2H^2}\rho$ at gridpoints in the computer RAM (random–access memory). Here $c = h$ for the 2^{nd} order scheme (94), and $c = 24h$ for the 4^{th} order scheme (100).

Calculation of $c\,\sigma_{i=j}$ from $c\,U_{k=l}$ using (134) requires *3 floating–point operations* $\times$ *2 or 3 components.*

Calculation of $c\,\sigma_{i\neq j}$ from $c\,U_{ij}$ and $c\,U_{ji}$ using (135) requires *6 floating–point operations* in 2-D and *18 floating–point operations* in 3-D.

Evaluation of $H^2 u_i''(\mathbf{x})$ from $c^2\,\sigma_{ij,j}$ using (136) requires *6 floating–point operations* in 2-D and *12 floating–point operations* in 3-D.

Finally, evaluation of (36) requires *3 additional floating–point operations per component.*

In total, staggered finite differences require *24 floating–point operations* plus evaluation of *8 partial schemes* in 2-D and *48 floating–point operations* plus evaluation of *18 partial schemes* in 3-D.

Evaluation of half–interval 2^{nd} order partial scheme of Section 6.7 costs *1 floating–point operation*, evaluation of half–interval 4^{th} order partial scheme of Section 6.8 costs *4 floating–point operations.* In general, evaluation of half–interval K^{th} order partial scheme costs *$-2+3K/2$ floating–point operations.*

The total number of floating–point operations per gridpoint, required to calculate the elastic wavefield in the next time instant using the staggered finite–difference scheme of the K^{th} order, is *$8+24K/2$ floating–point operations* in 2-D, or *$12+54K/2$ floating–point operations* in 3-D. For instance, the staggered finite differences of the 4^{th} order require *56 floating–point operations* per gridpoint in 2-D, and *120 floating–point operations* per gridpoint in 3-D.

12 Conclusions

The error analysis shows that, in smooth parts of the model, the most severe errors are due to the finite–difference approximation of the second space derivatives of the wavefield. Such errors cannot be reduced by applying some averaged "effective" material parameters. In this way, the application of purely point schemes inside geological blocks is justified.

For elastic waves in smooth parts of an isotropic medium, the fastest centred 2-D second–order finite–difference scheme is the scheme of Section 7.1, evaluating the mixed second partial wavefield derivatives by double application of the second–order 1-D scheme of Section 6.1. The fastest centred 3-D second–order scheme is its direct 3-D extension shown in Section 7.5.

Staggered second–order finite–difference schemes of Sections 7.10 (2-D) and 7.12 (3-D) are nearly twice faster than the centred second–order schemes, with the same accuracy for both P waves and S waves if ${v_\mathrm{P}}^2 \leq 3{v_\mathrm{S}}^2$, and with much better accuracy for slowly propagating S waves (${v_\mathrm{P}}^2 \gg 3{v_\mathrm{S}}^2$).

The best (both most accurate and fastest) centred 2-D fourth–order finite–difference scheme is the scheme of Section 7.4, evaluating the mixed second partial wavefield derivatives by double application of the fourth–order 1-D scheme of Section 6.2. The best centred 3-D fourth–order scheme is its direct 3-D extension shown in Section 7.8. The wavefield and the elastodynamic parameters are assumed to be differenced independently.

Staggered fourth–order finite–difference schemes of Sections 7.11 (2-D) and 7.13 (3-D) are about $\frac{3}{2}$ times faster than the centred fourth–order schemes, with $\frac{27}{32}$ times smaller error for both P waves and S waves if ${v_\mathrm{P}}^2 \le 3{v_\mathrm{S}}^2$, and with much better accuracy for slowly propagating S waves (${v_\mathrm{P}}^2 \gg 3{v_\mathrm{S}}^2$). The disadvantage of staggered fourth–order finite differences is their extent along a gridline, corresponding to the centred sixth–order scheme (in general, the size of the staggered scheme of the K^{th} order along a gridline is $2K-2$ grid intervals, which corresponds to the centred scheme of the $(2K-2)^{\mathrm{th}}$ order).

The fourth–order finite–difference schemes are undoubtedly superior to the second–order ones.

The relative phase–velocity error of the wave of a particular polarization and direction of propagation is given by (45), with its individual components derived in Sections 5.1, 7, 8, 9, and 10. In particular, the individual contributions to the relative phase–velocity error for the best centred 2-D and 3-D fourth–order spatial finite–difference schemes for the wavefield with the second–order time integration are given by equations (38), (125), (144) and (150), where error (125) due to the inaccurate second partial wavefield derivatives is dominant. This dominant error is given by (107) for the centred second–order finite differences, (125) for the centred fourth–order finite differences, (137) for the staggered second–order finite differences, and (139) for the staggered fourth–order finite differences.

Acknowledgements

The author is indebted to Heiner Igel, Ivan Pšenčík, and Jiří Zahradník for their essential comments and assistance during preparation of the final version of the manuscript.

The research has been supported by the Grant Agency of the Czech Republic under Contract 205/95/1465, and by the Institut Français du Pétrole, the Shell Research B.V., the Japan National Oil Corporation, and the Elf Geoscience Research Centre within the consortium project "Seismic Waves in Complex 3-D Structures".

References

Abramowitz, M. and Stegun, I.A. (1964), Handbook of Mathematical Functions. National Bureau of Standards, Washington D.C..

Alford, R.M., Kelly, K.R. and Boore, D.M. (1974), Accuracy of finite–difference modeling of the acoustic wave equation. Geophysics, **39**, 834–842.

Alterman, Z. and Karal, F.C. (1968), Propagation of elastic waves in layered media by finite–difference method. Bull. seismol. Soc. Am., **58**, 367–398.

Bickley, W.G. (1941), Formulae for numerical differentiation. Math. Gaz., **25**, 19–27.

Dablain, M.A. (1986), The application of high–order differencing to the scalar wave equation. Geophysics, **51**, 54–66.

Fornberg, B. (1988), Generation of finite difference formulas on arbitrary spaced grids. Math. Computation, **51**, 699–706.

Igel, H., Mora, P. and Riollet, B. (1995), Anisotropic wave propagation through finite–difference grids. Geophysics, **60**, 1203–1216.

Igel, H., Mora, P. and Rodrigues, D. (1991), 3-D wave propagation using finite differences. Expanded Abstracts, 61st Annual Int. SEG Meeting, pp. 1577–1579, Soc. Exploration Geophysicists, Tulsa.

Keller, H.B. and Pereyra, V. (1978), Symbolic generation of finite difference formulas. Math. Computation, **32**, 955–971.

Levander, A.R. (1988), Fourth–order finite–difference P-SV seismograms. Geophysics, **53**, 1425–1436.

Madariaga, R. (1976), Dynamics of an expanding circular fault. Bull. seismol. Soc. Am., **66**, 639–666.

Marfurt, K.J. (1984), Accuracy of finite–difference and finite–element modeling of the scalar and elastic wave equations. Geophysics, **49**, 533–549.

Sei, A. (1993), Computational cost of finite–difference elastic waves modeling. Expanded Abstracts, 63rd Annual Int. SEG Meeting, pp. 1065–1068, Soc. Exploration Geophysicists, Tulsa.

Stephen, R.A. (1988), A review of finite difference methods for seismo–acoustics problems at the seafloor. Rev. Geophys., **26**, 445–458.

Virieux, J. and Madariaga, R. (1982), Dynamic faulting studied by a finite difference method. Bull. seismol. Soc. Am., **72**, 345–369.

Virieux, J. (1986), P-SV wave propagation in heterogeneous media: Velocity–stress finite–difference method. Geophysics, **51**, 889–901.